Angular correlation distribution of electron-positron annihilation in graphite

1991 J. Phys.: Condens. Matter 3 2057

(http://iopscience.iop.org/0953-8984/3/13/008)

J. Phys.: Condens. Matter 3 (1991) 2057–2068. Printed in the UK

Angular correlation distribution of electron–positron annihilation in graphite

Lou Yongming,†§ B Johansson† and R M Nieminen‡

† Condensed Matter Theory Group, Physics Department, Uppsala University, Box 530, S-75121, Uppsala, Sweden

‡ Laboratory of Physics, Helsinki University of Technology, SF-02150 Espoo, Finland

§ Physics Department, Tsinghua University, Beijing, People's Republic of China

Received 13 September 1990, in final form 14 January 1991

Abstract. Using the empirical pseudopotential method for the electron wavefunction and the variational positron wavefunction, we have calculated the one- and two-dimensional angular correlation distribution of electron–positron annihilation (ACAR) as well as the electron momentum distribution (EMD) for graphite. The calculated ACAR as well as its anisotropy are in good agreement with experiments. Due to the presence of the positron, the calculated ACAR shows stronger anisotropy than the corresponding EMD, which is in agreement with the experimental data. It is shown that the layer structure of graphite is more clearly exhibited by the ACAR than the EMD. The remaining discrepancy between the presently calculated ACAR distribution and the experimental spectra is discussed and it is argued that it originates from the quality of the single-crystal sample used in the experiments and the electron–positron many-body interaction which has not been included in our theoretical treatment.

1. Introduction

The electronic structure of graphite has been the subject of intensive experimental and theoretical studies [1–22]. This interest is partly due to the fact that graphite can be considered as a prototype for quasi-two-dimensional materials. Graphite exhibits strong anisotropy in many of its physical properties, which may be understood in terms of its layered hexagonal crystal structure. For relatively recent reviews of the electronic energy band structure of graphite the reader is referred to [1] and [2]. While the ground-state energy band structure has been established experimentally by angle-resolved photoemission spectroscopy [8–13] and found to be in good agreement with the theoretical work [1–7], the unoccupied band structure is still a matter of discussion both theoretically and experimentally [21]. Here we will focus our interest on the electron momentum distribution (EMD) as well as on the angular correlation distribution of electron–positron annihilation (ACAR), which is the electron momentum distribution sampled by the positron.

Compton scattering of x- and γ-rays has been successfully applied to determine the electron momentum distribution (EMD) for a number of materials [23, 24]. Also, for graphite, the Compton profile has been measured and calculated by a number of groups [25–34] in order to investigate the EMD and its anisotropy. Since the Compton profile

0953-8984/91/132057 + 12 $03.50

only measures the one-dimensional electron momentum distribution, many previous theoretical calculations on graphite have dealt with the one-dimensional EMD. Both the measured and the calculated anisotropy of the Compton profile are considerably smaller than what one would at first expect from the layer structure of graphite and are also smaller than the anisotropy of the corresponding angular correlation distribution in positron annihilation experiments [35–38]. There are, however, several reasons for these unexpectedly small anisotropies of the Compton profile. Among them, the mosaic spread of the crystal samples causes a substantial reduction of the anisotropy of the profile [32]. In spite of that the one-dimensional EMD shows a relatively small anisotropy, theoretical work shows that the two-dimensional EMD is strongly anisotropic and the layer structure is clearly exhibited. This has been discussed in detail elsewhere [34]. However, the higher-dimensional EMD cannot be observed directly. It is only after a reconstruction of experimental Compton profiles or a reconstruction of the experimental ACARs after removing the positron contribution that the higher-dimensional EMD can be obtained.

In the last decade, the positron annihilation technique has developed rapidly [39]. Unlike Compton scattering, the two-dimensional angular correlation distribution of the electron–positron annihilation (ACAR) can be measured directly and has become well established as a tool in the investigation of electron momentum distribution [39]. Interestingly enough the two-dimensional ACAR of graphite shows a strong anisotropy [40, 41]. Despite that several experimental ACAR spectra [35–38, 40–42] have been reported, there is still a lack of theoretical calculations explaining the observed spectra, especially for the two-dimensional ACAR. Besides the possibility of using graphite as an example to study the relationship between ACAR and EMD, the lower electron density in the interlayer region makes it also an interesting system for investigation of the electron–positron many-body interaction or enhancement factor [43]. Graphite exhibits probably the largest difference between the ACAR spectra and the Compton profile that has so far been reported. This is in sharp contrast to diamond where the ACAR and Compton profile are quite similar to each other [26], a fact which stresses the importance of the layer structure of graphite. Therefore graphite becomes a most important material to be investigated by means of the Compton profile and the ACAR techniques.

In the present study, we will concentrate on the anisotropy of the ACAR and its connection to the electron momentum distribution. Using the electron wavefunction calculated from the empirical pseudopotential method (EPM) and the variational positron wavefunction, we have calculated the one- and two-dimensional angular correlation distributions of the electron–positron annihilation (ACAR) for graphite. The calculated ACAR as well as its anisotropy are in good agreement with experiments. Below we will also demonstrate that the layer structure of graphite is more clearly exhibited by the ACAR than by the EMD.

2. Theoretical calculations

The pseudopotential formalism has become a well established method to investigate the electronic structure of s–p bonded materials [44, 45]. The reader is referred to [44, 45] for details of the formalism. Van Haeringen and Junginger [46] have used this method to calculate the energy band of graphite and their over-all results are in reasonably good agreement with experiment. Holzwarth *et al* [2] have also used the pseudopotential technique and the local density functional approximation together with a mixed basis

set of plane waves and linear combinations of atomic orbitals to calculate the energy bands of graphite. The results of the occupied bands in graphite are in good agreement with other calculations and with angle-resolved photoemission experiments [8]. The unoccupied band structure is closer to the experiments of angle-resolved inverse photoemission spectroscopy (ARIPES) than other previous calculations although some disagreement still exists between the calculation and experimental data [21, 22]. We choose the pseudopotential form factor parameters from curve 1 in [28] to calculate the electron wavefunction. The calculated energy bands are in general good agreement with the theoretical result of [2], and the calculated Compton profile compares well with the theoretical results of Chou *et al* [33] which are discussed in detail elsewhere [34].

Following Chiba *et al* [47, 48], the variational positron wavefunction $\Psi_+(r)$ (for $k = 0$) is written as

$$\Psi_+(r) = 1 - \sum_i \exp(-\alpha|r - R_i|^2) \tag{1}$$

where R_i is the position of the ith ion in a unit cell. The variational parameter α is determined to minimize the ground-state energy. Here we take the value $\alpha = 0.5$ from [37].

The angular correlation distribution of electron–positron annihilation (ACAR) $\rho^{2\gamma}(p)$ is given by

$$\rho^{2\gamma}(p) = \sum_{n,k}^{\text{occ}} \left| \int dr \exp(-ip \cdot r)\Psi_{n,k}(r)\Psi_+(r) \right|^2 \tag{2}$$

where $\Psi_{n,k}$ is the electron wavefunction for an electron in the nth band with wave vector k inside the first Brillouin zone. The electron wavefunction and the positron wavefunction can be expanded as, respectively,

$$\Psi_{n,k}(r) = \sum_G^{\text{all}} C_{n,-G}(k) \exp[i(k - G) \cdot r] \tag{3}$$

$$\Psi_+(r) = \sum_Q^{\text{all}} B(Q) \exp[iQ \cdot r] \tag{4}$$

where G and Q are the reciprocal lattice vectors. We then obtain

$$\begin{aligned}\Phi(p) &= \int dr \exp(-ip \cdot r)\Psi_{n,k}(r)(r)\Psi_+(r) \\ &= \sum_G^{\text{all}} \sum_Q^{\text{all}} C_{n,-G}(k)B(Q)\delta(k - p - G + Q) \\ &= \sum_G^{\text{all}} C_{n,-G}(k)B(p + G - k)\end{aligned} \tag{5}$$

and

$$\rho^{2\gamma}(p) = \sum_{n,k}^{\text{occ}} \left| \sum_G^{\text{all}} C_{n,-G}(k)B(p + G - k) \right|^2. \tag{6}$$

In our calculations we have included 581 reciprocal lattice vectors in the summation of (3), (4) and (6). The two-dimensional ACAR is obtained from

$$I(p_x, p_y) = \int \rho^{2\gamma}(p)\, dp_z. \tag{7}$$

The one-dimensional ACAR is obtained from $\rho^{2\gamma}(\boldsymbol{p})$ by the following double integral

$$J(p_z) = \iint \rho^{2\gamma}(\boldsymbol{p})\, \mathrm{d}p_x\, \mathrm{d}p_y. \tag{8}$$

3. Results and discussions

In figure 1 we show the calculated one-dimensional ACAR distribution J_{0001} along the c axis [0001] direction and also the distribution J_{xy} averaged over the xy basal plane and compare with corresponding experimental distributions of [36]. Our results are in

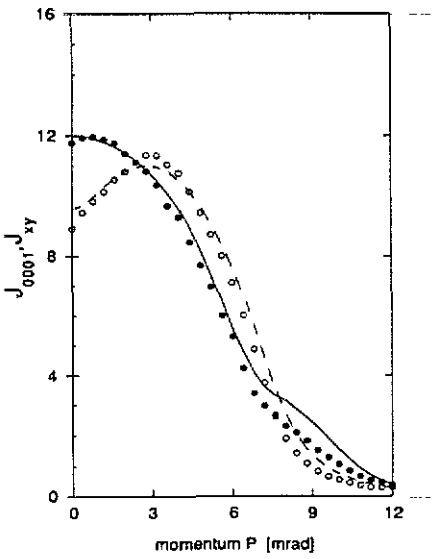

Figure 1. One-dimensional angular correlation distribution (ACAR) for graphite. The broken and full curves are the present calculations. The open and full circles are the experimental results from [36]. The broken curve and open circles represent the ACAR J_{0001} along the [0001] direction. The full curve and full circles represent the ACAR J_{xy} averaged over the xy basal plane.

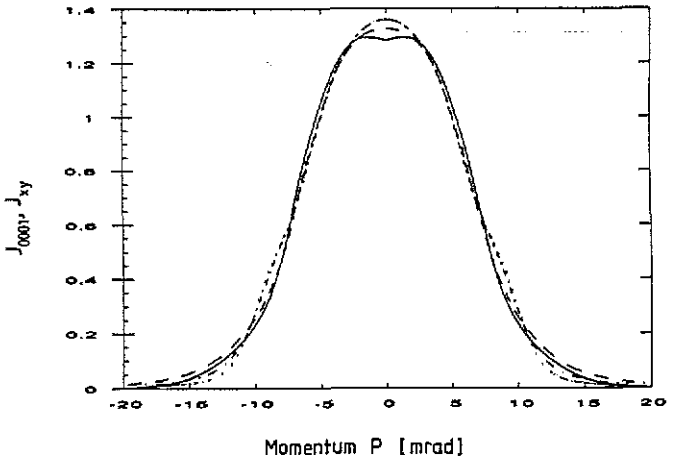

Figure 2. Directional Compton profiles for graphite. The dotted and full curves are the present calculations. The chain and broken curves are the theoretical results from [33]. The dotted and chain curves represent the J_{xy} profile averaged over the xy basal plane. The broken and full curves represent the J_{0001} profile along the [0001] direction.

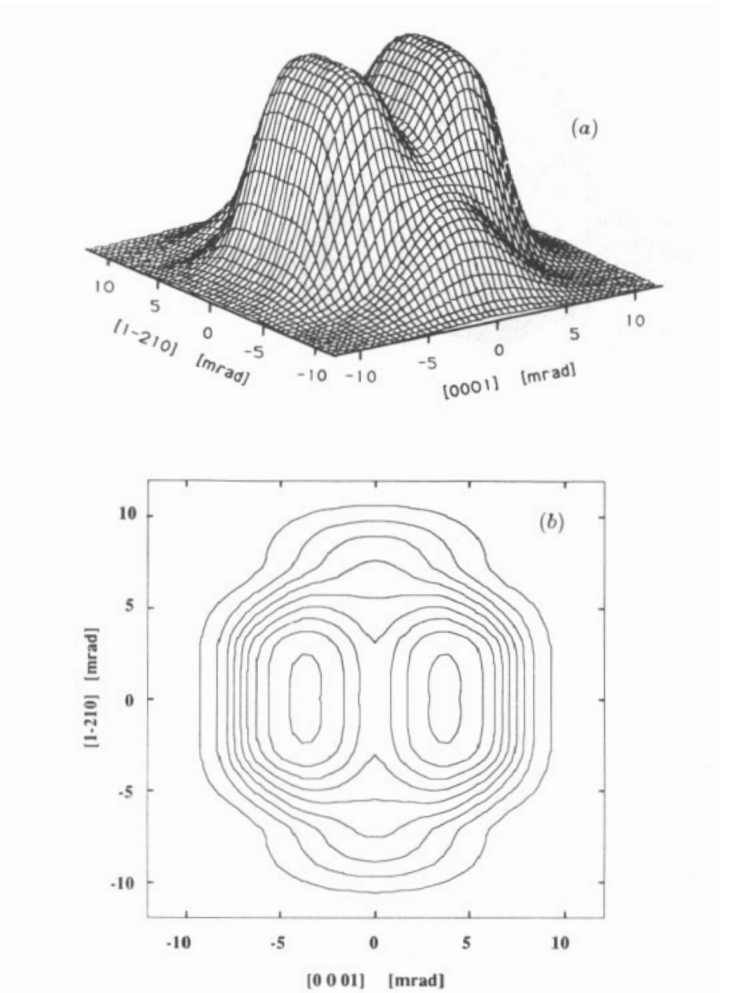

Figure 3. (*a*) The two-dimensional angular correlation distribution (ACAR) $I(p_y, p_z)$ of graphite integrated along the [1 0 −1 0] direction; $p_y \| [1\ -2\ 1\ 0]$ and $p_z \| [0001]$. (*b*) calculated contour plot of $I(p_y, p_z)$.

general agreement with the experimental data, especially for the distribution J_{0001} along the c axis [0001] direction. For the distribution J_{xy}, the structure (i.e. the deviation from the Gaussian shape) between 7–11 mrad in the theoretical distribution is more pronounced than observed experimentally. There are several reasons for this difference, such as the lack of a high quality single crystal, the electron–positron many-body interaction as well as the inaccuracy of the simple variational positron wavefunction. If the electron–positron many-body interaction plays the same role for both the direction distributions J_{0001} and J_{xy}, the difference between the theoretical and experimental J_{xy} is most likely mainly due to the lack of quality of the single crystal. The lack of quality of the single crystal has forced all the previous experiments to be carried out on highly oriented pyrolytic graphite (HOPG). As it does for the Compton profile [32], the mosaic spread will certainly reduce the structure between 7–11 mrad. In [32] it was shown that

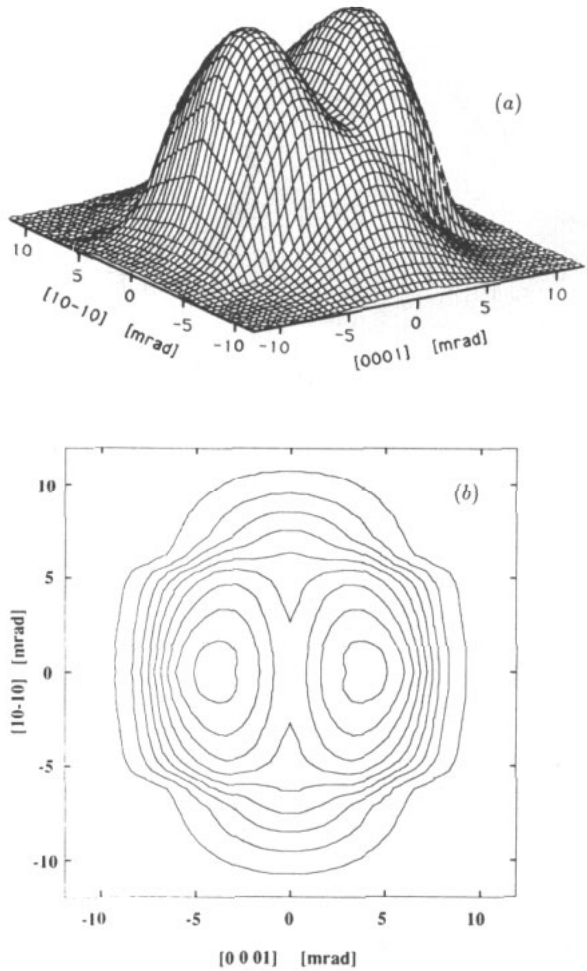

Figure 4. (*a*) The two-dimensional angular correlation distribution (ACAR) $I(p_z, p_x)$ of graphite integrated along the [1 −2 1 0] direction; $p_x \| [1\,0\,-1\,0]$ and $p_z \| [0001]$. (*b*) calculated contour plot of $I(p_z, p_x)$.

the 53° mosaic spread of the graphite sample used in the experiment reduces the maxima and minima of the anisotropy of the Compton profile by 25%. In [37] the ACAR structure between 7–11 mrad is much less pronounced than in [36] indicating differences in sample quality. The mosaic spread of the *c* axis is more difficult to deal with in the theoretical calculation than a completely random distribution in the basal plane. The nature of HOPG makes a detailed comparison between the experiment and theory somewhat inconclusive and therefore it is not possible to obtain a firm conclusion on the electron–positron many body enhancement which depends heavily on a detailed comparison between experiment and theory.

Our calculated directional Compton profiles J_{0001} along the *c* axis [0001] direction and also the distribution J_{xy} averaged over the *xy* basal plane are shown in figure 2 together with the theoretical profiles from [33]. It can be clearly seen that the anisotropy

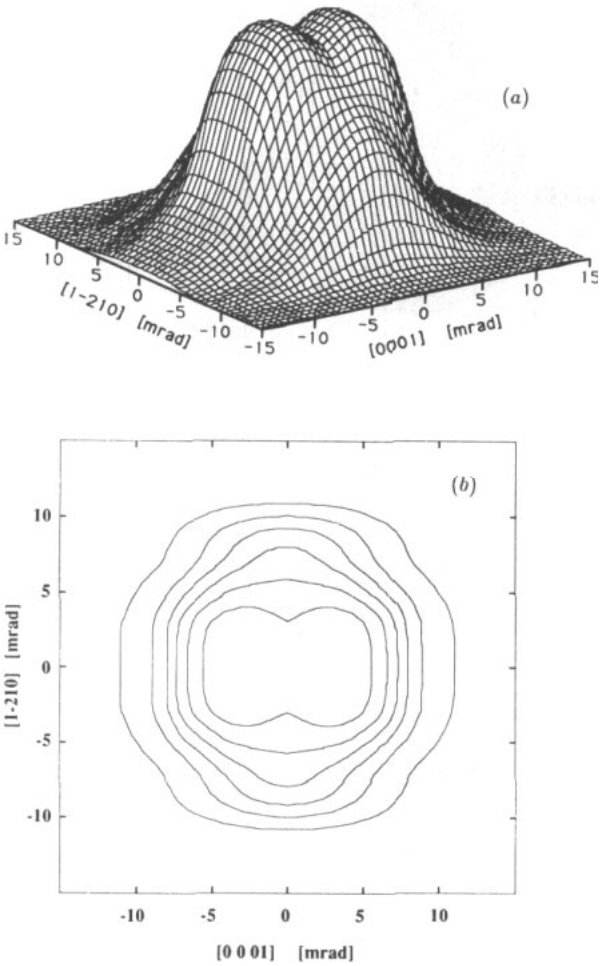

Figure 5. (*a*) The two-dimensional electron momentum distribution (EMD) $I(p_y, p_z)$ of graphite integrated along the [1 0 −1 0] direction; $p_y \| [1\ -2\ 1\ 0]$ and $p_z \| [0001]$. (*b*) calculated contour plot of $I(p_y, p_z)$.

in the ACAR is much larger than in the Compton profile. In addition the ACAR distribution is much narrower than the Compton profile. These differences for graphite between the Compton profiles and the ACAR of positron annihilation arise for the following reasons: (i) the Coulomb perturbation on the wavefunction of the annihilated electron by the positron [35, 36, 40]; (ii) the positron preferring to stay in the interlayer region, where the electron density is lower and the local electron momentum distribution is narrower than the averaged bulk values; (iii) the details of the positron wavefunction [35, 36, 40]. Unlike reasons (ii) and (iii) which have been taken into account in the present calculation, the Coulomb perturbation from the positron on the electron wavefunction is rather difficult to treat because the effective density of the delocalized positron will be nearly zero due to the fact that there is only one single positron present. Usually it is taken into account through the many-body enhancement factor. As discussed above, the lack of a

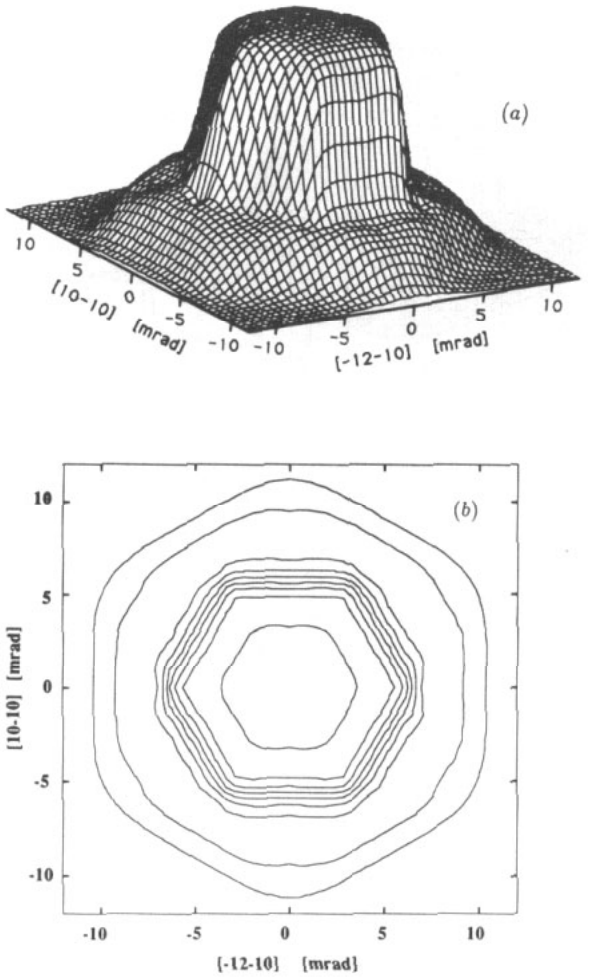

Figure 6. (*a*) The two-dimensional angular correlation distribution (ACAR) $I(p_x, p_y)$ of graphite integrated along the [0001] direction, $p_x \| [1\,0\,-1\,0]$ and $p_y \| [-1\,2\,-1\,0]$. (*b*) calculated contour plot of $I(p_x, p_y)$.

large single crystal and therefore less precise data makes an experimental estimation of the enhancement very difficult. When high quality and large single crystal graphite becomes available, it will provide an interesting possibility to investigate the electron–positron many-body enhancement factor in the lower electron density region. Probably the effect can also be treated by the recently proposed PEP (positron–electron product) formalism, in which the positron–electron product wavefunction is obtained from a wave equation. This, however, requires that the normalization constant and other problems inherent in the PEP formalism have been solved [49, 50]. Since the positron prefers to stay in the interlayer region, it will tend to favour annihilation with π electrons rather than σ electrons. It is known that the EMD of σ electrons is quite isotropic, while the EMD of π electrons is highly anisotropic. The preferential annihilation of the positron

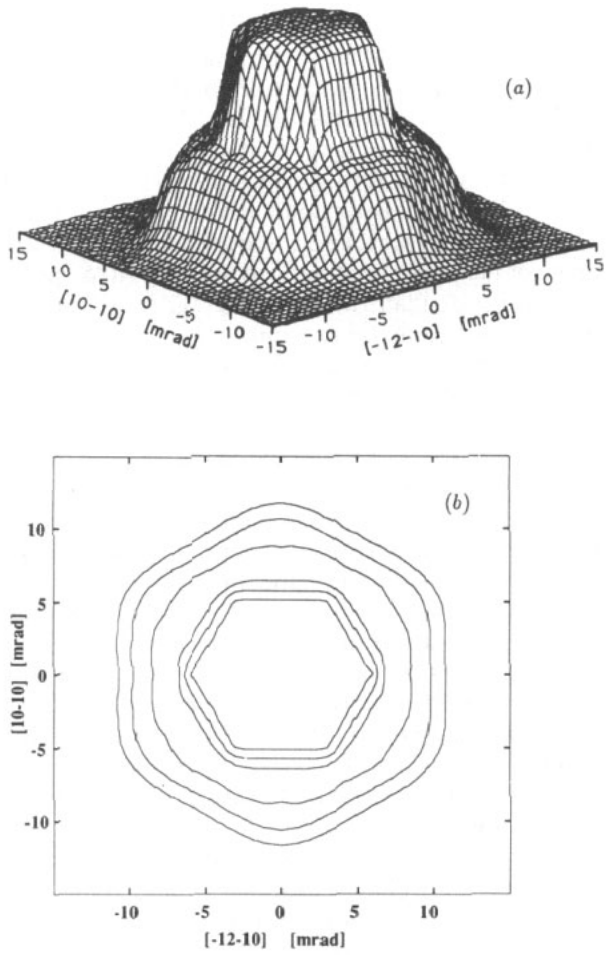

Figure 7. (*a*) The two-dimensional electron momentum distribution (EMD) $I(p_x, p_y)$ of graphite integrated along the [0001] direction; $p_x \| [1\,0\,-1\,1]$ and $p_y \| [-1\,2\,-1\,0]$; (*b*) calculated contour plot of $I(p_x, p_y)$.

with the π electron is the reason why the anisotropy of the ACAR is more pronounced than it is for the Compton profile. For the same reason, i.e. the preferential annihilation in the interlayer region and the narrow local EMD in the interlayer region, the ACAR is much narrower than the corresponding Compton profile.

The remaining difference between our present calculations and the experimental profiles can be reduced by the following procedures: (i) using a more accurate positron wavefunction; (ii) including the electron–positron many-body enhancement factor; (iii) using a single crystal of graphite in the ACAR experiment. It would be of great help if a variety of experimental data were available for single-crystal graphite instead of HOPG. At present there are only a few experiments, such as ARIPES measurements [21, 22], performed on single-crystal graphite.

The two-dimensional ACAR integrated along the [1 0 −1 0] direction is shown in figure 3(*a*). Figure 3(*b*) shows contours of the same data as (*a*). The distribution is of a bimodal form with a saddle point at $(p_{1\text{-}210}, p_{0001}) = (0, 0)$ which is in agreement with the experimental distribution [40] of HOPG except that the shape of the peaks along the direction perpendicular to the *c* axis is broader than the experimental data. The difference in the shape of the peaks is not surprising since in the experiment the basal plane of HOPG is randomly oriented. A similar two-dimensional ACAR integrated along the [1 −2 1 0] direction is shown in figure 4(*a*), and contours of the same data are shown in figure 4(*b*). Now, the shape of the peaks becomes narrower, even to the extent that they are now even somewhat narrower than the experimental two-dimensional ACAR of HOPG. It is expected that the experimental two-dimensional ACAR of HOPG would lie between the distribution of figure 3 and figure 4. The two-dimensional ACAR integrated along the [1 0 −1 0] direction is similar to the corresponding two-dimensional EMD shown in figure 5 but has a narrower distribution and a much deeper valley at the centre of the distribution. Similar to the 2D EMD [34], the bimodal shape of 2D ACAR is caused by the layer structure of graphite, which will be discussed further below.

In figures 6(*a*) and (*b*) we show the two-dimensional ACAR integrated along the *c* axis [0001] direction and its contours, respectively. The layer structure can now be clearly seen. In the central part of the Brillouin zone, the amplitude of the two-dimensional ACAR is almost constant and has hexagonal symmetry. Near the first Brillouin zone faces ⟨1 0 −1 0⟩, the amplitude of the two-dimensional ACAR drops sharply to about one-third of its maximum value. For semimetals, semiconductors or insulators this might be a typical feature of layer structures with large layer separations. As for the corresponding 2D EMD and its contours shown in figures 7(*a*) and (*b*), respectively [34], the central plateau in the distribution is caused by a strong potential parameter along the *c* axis direction which gives rise to a strong correlation between the wavefunction with wave vector $\boldsymbol{k}$ in the first Brillouin zone and the wavefunction with wave vector $\boldsymbol{G}_{\langle 0002\rangle} - \boldsymbol{k}$ in the higher zone directly above or below the first Brillouin zone, i.e. $\Psi(\boldsymbol{k})$ and $\Psi(\boldsymbol{G}_{\langle 0002\rangle} - \boldsymbol{k})$. This holds for both the electron and positron wavefunctions. The sharp drop in the distribution is caused by the strong correlation between the wavefunction $\Psi(\boldsymbol{k})$ and the wavefunction $\Psi(\boldsymbol{G}_{\langle 10\text{-}10\rangle} - \boldsymbol{k})$ near the Bragg plane $\boldsymbol{G}_{\langle 10\text{-}10\rangle}/2$. If the layer spacing *c* is small, the corresponding potential parameters $U(\boldsymbol{G})$ with $\boldsymbol{G}$ along the [0001] direction will also be small and there will not be such a feature in the two-dimensional EMD as well as ACAR, i.e. the plateau in the central part of the Brillouin zone and the sharp drop near the first Brillouin zone face $\boldsymbol{G}_{\langle 10\text{-}10\rangle}/2$. The presence of the positron makes the decrease of the ACAR larger than the decrease of the EMD, e.g. a decrease to one-third of its maximum in ACAR compares with a decrease to one-half of its maximum in EMD. Based on the investigation of the 2D EMD in [34] and the experimental 2D ACAR on graphite as well as potassium-intercalated graphite [40, 41], we suspect that graphite is not a unique case in showing such a layer structure in its two-dimensional ACAR. It would be interesting to see if future experiments of the corresponding two-dimensional ACAR integrated along [0001] will confirm this assessment.

Like the Compton profile measurements, the positron experiments also suffer from the lack of large single crystals of graphite. It is found, using a sample stacked by four fairly good single crystals, that the measured two-dimensional ACAR [42] is markedly different than the results [40] from the HOPG sample. At present, data are not available for the two-dimensional ACAR integrated along the [0001] direction. It might, however, soon become available together with other differently oriented two-dimensional ACAR measurements from higher quality single-crystal samples than before [51]. It would be

valuable if the Compton profile and the ACAR of the positron annihilation were studied jointly on the same sample and that also the reconstruction of the two- and three-dimensional EMD from the Compton profile and the reconstruction of the three-dimensional ACAR from the two-dimensional ACAR could be done together. This would provide a possibility for a unified understanding of the EMD and ACAR as well as the electron wavefunction for graphite and perhaps also for other layer structure materials.

4. Conclusion

We have calculated the one- and two-dimensional angular correlation distribution of electron–positron annihilation (ACAR) as well as the electron momentum distribution (EMD) for graphite. The calculated ACAR as well as the anisotropy are in good agreement with experiments. Due to the presence of the positron, the calculated ACAR shows stronger anisotropy than its corresponding EMD, which is again in agreement with the experimental data. A comparison is made for the EMD and ACAR of graphite. It is shown that the layer structure of graphite is more clearly exhibited by the ACAR than the EMD. We have suggested a new oriented 2D ACAR integrated along the [0001] direction to be measured, which is more similar to the corresponding 2D EMD than the other oriented two-dimensional distribution. The remaining discrepancy between the calculated ACAR distribution and the experimental spectra has been discussed. The quality of the single-crystal sample and the electron–positron many-body interaction are most likely to be responsible for the deviation between theory and experiment. The comparison between the theoretical ACAR and the experimental ACAR from a single crystal together with its relation to the corresponding EMD of Compton experiments deserve further investigation for graphite as well as for other layer structure materials. Graphite appears to be a well-suited and interesting system for investigating the reconstruction of the three-dimensional ACAR and its connection with the three-dimensional EMD.

Acknowledgment

Lou Yongming and B Johansson would like to acknowledge the Swedish Natural Science Research Council (NFR) for financial support.

References

[1] Tatar R C and Rabii S 1982 *Phys. Rev.* B **25** 4126
[2] Holzwarth N A W, Louie S G and Rabii S 1982 *Phys. Rev.* B **26** 5382
[3] Mallet C P 1981 *J. Phys. C: Solid State Phys.* **14** L213
[4] Zunger A 1978 *Phys. Rev.* B **17** 626
[5] Willis R F, Fitton B and Painter G S 1974 *Phys. Rev.* B **9** 1926
[6] Posternak M, Balderschi A, Freeman A J, Wimmer E and Weinert M 1983 *Phys. Rev. Lett.* **50** 761
[7] Posternak M, Balderschi A, Freeman A J and Wimmer E 1984 *Phys. Rev. Lett.* **52** 863
[8] Eberhardt W, McGovern I T, Plummer E W and Fischer J E 1980 *Phys. Rev. Lett.* **44** 200
McGovern I T, Eberhardt W, Plummer E W and Fischer J E 1980 *Physica* **99B** 415
[9] Law A R, Barry J J and Hughes H P 1983 *Phys. Rev.* B **28** 5332
[10] Marchand D, Frétigny C, Laguës M, Batallan F, Simon Ch, Rosenman I and Pinchaux R 1984 *Phys. Rev.* B **30** 4788
[11] Law A R, Johnson M T and Hughes H P 1986 *Phys. Rev.* B **34** 4289

[12] Pescia D, Law A R, Johnson M T and Hughes H P 1985 *Solid State Commun.* **56** 809
[13] Takahashi T, Tokailin H and Sagawa T 1985 *Phys. Rev.* B **32** 8317
[14] Law A R, Johnson M T, Hughes H P and Padmore H A 1985 *J. Phys. C: Solid State Phys.* **18** L297
Johnson M T, Law A R and Hughes H P 1985 *Surf. Sci.* **162** 11
[15] Papagno L and Caputi L S 1983 *Surf. Sci.* **125** 530
[16] Fauster Th, Himpsel F J, Fisher J E and Plummer E W 1983 *Phys. Rev. Lett.* **51** 430
[17] Reihl B, Gimzewski J K, Nicholls J M and Tosatti E 1986 *Phys. Rev.* B **33** 5770
[18] Schäfer I, Schüter M and Skobowski M 1987 *Phys. Rev.* B **35** 7663
[19] Ohsawa H, Takahashi T, Kinoshita T, Enta Y, Ishii H and Sagawa T 1987 *Solid State Commun.* **61** 347
Maeda F, Takahashi T, Ohsawa H and Suzuki S 1988 *Phys. Rev.* B **37** 4482
[20] Dittmar-Wituski A, Naparty M and Skonieczny J 1985 *J. Phys. C: Solid State Phys.* **18** 2563
[21] Claessen R, Cartstensen H and Skobowski M 1988 *Phys. Rev.* B **38** 12582
[22] Collins I R, Andrews P T and Law A R 1988 *Phys. Rev.* B **38** 13348
[23] 1977 *Compton Scattering* ed B G Williams (New York: McGraw-Hill)
[24] Cooper M J 1985 *Rep. Prog. Phys.* **48** 415
[25] Cooper M and Leake J A 1967 *Phil. Mag.* **5** 1201
[26] Weies R J and Phillips W C 1968 *Phys. Rev.* **176** 900
[27] Paakkari T L P 1974 *Phys. Fenn.* **9** 185
[28] Reed W A, Eisenberger P, Pandey K C and Snyder L C 1974 *Phys. Rev.* B **10** 1507
[29] Dovesi R, Pisani C, Roetti C and Dellarole P 1981 *Phys. Rev.* B **24** 4170
[30] Vasudevan S, Rayment T, Williams B G and Holt R 1984 *Proc. R. Soc.* A **391** 109
[31] Loupias G, Chomilier J and Guérard D 1984 *J. Phys. Lett. Paris* **45** L301; 1985 *Solid State Commun.* **55** 299
[32] Tyk R, Felsteiner J, Gertner I and Moreh R 1985 *Phys. Rev.* B **32** 2625
[33] Chou M Y, Marvin L, Cohen L and Louie S G 1986 *Phys. Rev.* B **33** 6619
[34] Lou Yongming, Johnsson B and Nieminen R M 1991 *J. Phys.: Condens. Matter* **3** 1699
[35] Berko S, Kelley R E and Plaskett J S 1957 *Phys. Rev.* **106** 824
[36] Cartier E, Heinrich F, Gubler U M, Pfluger P, Geiser V and Güntherodt H-J 1983 *Synthetic Metals* **8** 119
[37] Shimotomai M, Iwata T, Takahashi T and Doyama M 1983 *J. Phys. Soc. Japan* **52** 694
[38] Colombino P, Fiscella B and Trossi L 1963 *Nuovo Cimento* **27** 589
[39] See, for example Berko S 1983 *Positron Solid State Physics* eds W Brandt and A Dupasquier (New York: North-Holland) p 64
Mijnarends P E 1983 *ibid* p 146
[40] Lee R R, von Stetter E C, Hasegawa M and Berko S 1987 *Phys. Rev. Lett.* **58** 2363
[41] Sferlazzo P, Berko S, Lynn K G, Mills A P Jr, Roellig L O, Viescas A J and West R N 1988 *Phys. Rev. Lett.* **60** 538
[42] Kanazawa I, Tanigawa S, Suzuki R, Mizuhara Y, Sano M and Inokuchi H 1987 *J. Phys. Chem. Solids* **48** 701
[43] Jarlborg T private communication
[44] 1966 *Pseudopotentials in The Theory of Metals* ed W A Harrison (New York: Benjamin)
[45] 1970 *Solid State Physics* vol 24 ed H Ehrenreich, F Seitz and D Turnbull (New York: Academic Press)
[46] van Haeringen W and Junginger H G 1969 *Solid State Commun.* **7** 1723
[47] Chiba T and Tsuda N 1974 *Appl. Phys.* **5** 37
[48] Chiba T 1976 *J. Chem. Phys.* **64** 1182
[49] Lou Yongming, Nieminen R M and Johansson B 1991 *J. Phys.: Condens. Matter* **3** 163
[50] Lou Yongming, Johansson B and Nieminen R M 1991 *Phys. Scripta* **43** 123
[51] Tanigawa S private communication